

Image Dehazing with Hybrid ℓ_2 - ℓ_0 Penalty Mode

Yuxuan Zhou, Dongjiang Ji*, Chunyu Xu

School of Science, Tianjin University of Technology and Education, Tianjin, China

Email: *zjkjdj@tute.edu.cn

How to cite this paper: Zhou, Y.X., Ji, D.J. and Xu, C.Y. (2024) Image Dehazing with Hybrid ℓ_2 - ℓ_0 Penalty Mode. *Journal of Computer and Communications*, 12, 132-152. <https://doi.org/10.4236/jcc.2024.1210010>

Received: September 27, 2024

Accepted: October 22, 2024

Published: October 25, 2024

Copyright © 2024 by author(s) and Scientific Research Publishing Inc. This work is licensed under the Creative Commons Attribution International License (CC BY 4.0). <http://creativecommons.org/licenses/by/4.0/>



Open Access

Abstract

Due to the presence of turbid media, such as microdust and water vapor in the environment, outdoor pictures taken under hazy weather circumstances are typically degraded. To enhance the quality of such images, this work proposes a new hybrid ℓ_2 - ℓ_0 penalty model for image dehazing. This model performs a weighted fusion of two distinct transmission maps, generated by imposing ℓ_2 and ℓ_0 norm penalties on the approximate regression coefficients of the transmission map. This approach effectively balances the sparsity and smoothness associated with the ℓ_0 and ℓ_2 norms, thereby optimizing the transmittance map. Specifically, when the ℓ_2 norm is penalized in the model, an updated guided image is obtained after implementing ℓ_0 penalty. The resulting optimization problem is effectively solved using the least square method and the alternating direction algorithm. The dehazing framework combines the advantages of ℓ_2 and ℓ_0 norms, enhancing sparse and smoothness, resulting in higher quality images with clearer details and preserved edges.

Keywords

Atmospheric Scattering Model, Guided Filter with ℓ_2 Norm, ℓ_0 Gradient Minimization, Single Image Dehazing, Transmission Map, Ridge Regression

1. Introduction

Larger particles alter light absorption, emission, and scattering in the atmosphere, which are the primary cause of natural phenomena including haze, smoke, and fog. The quality of images taken in haze weather is significantly degraded: clarity, contrast, and visibility are greatly reduced, the image details are blurred, and color

deviation and distortion are produced [1]. Therefore, it is crucial to remove the undesired blurred visual effects from the captured images. The dehazing algorithm plays an important role in it and it can be broadly categorized into two categories: one is based on image enhancement and the other is based on image restoration.

The image enhancement method focuses on reducing specific information in the image based on particular needs. It involves processing image features such as contrast, edges, and contours to enhance visual appearance. However, this method does not prioritize image fidelity or consider the physical causes behind the image characteristics. Techniques in this category include histogram equalization [2] [3], which expands the dynamic range to boost image contrast. The homomorphic filtering proposed by Stockman [4] enhances the image contrast by enhancing the high-frequency components and weakening the low-frequency components. Image enhancement based on wavelet is similar to homomorphic filtering, and Russo [5] uses wavelet transform to equalize images and gets good results. Retinex [6] proposed by Land enhanced the image by eliminating the influence of the reflection component in the image, which was improved by later Jobson and Rahman, who proposed Single Scale Retinex and Multi Scale Retinex [7] [8].

The physical model-based dehazing approach, also known as the image restoration-based haze removal method, builds a model of hazy picture degradation by investigating the causes of hazy image degradation and addresses the inverse process of image degradation to restore clear images. Fattal *et al.* [9] posited that there is no correlation between scene transmission and surface shading in their hypothesis. They used the independent component analysis (ICA) algorithm combined with a Markov random field model to estimate scene transmission. However, this method often falls short in conditions of dense haze. Tan *et al.* [10] improved the local contrast of hazy images using a Markov random field model, restoring some texture and structure but frequently over-enhancing the contrast. Tarel *et al.* [11] proposed a method of dehazing using median filtering to estimate atmospheric map and transmission map, which requires less processing time, but often has poor processing results for images with dense haze. A dehazing approach suited for vast sky regions has been proposed by Meng *et al.* [12], and the transmission map was estimated using the boundary constraint hypothesis and contextual optimization. While the method effectively removes haze, it tends to distort objects whose colors resemble atmospheric light. Li *et al.* [13] introduced a weighted guided image filter for dehazing, which reduces halo artifacts in both flat and sharp regions while preserving edge information more effectively. However, this approach still results in over-smoothing in sharp areas due to the use of a local linear model and a fixed regularization parameter. Additionally, Li *et al.* [14] proposed an efficient single image haze removal approach based on edge-preserving decomposition, and the edge-preserving smoothing method is used to estimate the transmission map. However, the over-smoothing effect persists in the sharp regions. To address this, some global optimization-based filters like the weighted

least square (WLS) [15] and fast weighted least square (FWLS) [16] have been introduced. These techniques avoid the edge-smoothing effect but are more time-consuming due to the increased number of iterations required. Zhu *et al.* [17] proposed a fusion-based algorithm for solving the image dehazing problem without considering the degradation mechanism. They utilized the guide filter to decompose the unexposed image into local and global components. The method offers several advantages, including computational efficiency, clear detail, good color quality, and satisfactory results. Raikwar *et al.* [18] rearranged the atmospheric scattering model to estimate the transmission map by calculating the difference of minimum color channels. This approach aims to enhance visibility restoration. Similarly, Zhao *et al.* [19] developed a single image dehazing method that analyzes the prior information of local dehazed patches. They accurately estimated the transmission based on these local patches. To improve the quality of the transmission map, they applied weighted interpolation and guided filtering to enhance the edges and details. P.S. Baiju *et al.* [20] proposed an optimization framework using weighted kernel norm minimization, which preserves prominent edges and detailed structures to obtain a finer transmission map. A scale-aware weighting-based effective edge-preserving gradient domain guided image filter was proposed by Yadav *et al.* [21], in which sharp and flat regions retained edge information while removing image artifacts. Padmini *et al.* [22] proposed a method of ℓ_0 smoothing after guided filtering. Still, this method can't remove pixel-clustering artifacts, so Joongchol Shin *et al.* [23] present a new structure-guided ℓ_0 -norm that removes various artifacts while counting the global gradients of an image.

He *et al.* [24] proposed a dehazing algorithm based on dark channel priors; and improved the transmission map using soft matting, resulting in clearer restored images. However, this approach had a large computational cost and exhibited gradient reversal and halo artifacts in smooth and sharp regions. To address these issues, He *et al.* [25] introduced guided filtering with ℓ_2 norm penalty as an alternative to soft matting. This optimization reduced the algorithm's complexity, mitigated artifact problems, and enhanced the naturalness of the dehazing effect. However, the use of ℓ_2 norm penalty may hinder the retention of edge information in sharp regions. Xu *et al.* [26] proposed using the ℓ_0 gradient minimization model for image processing. The model optimizes the sparsity of gradient by controlling the number of non-zero gradients, resulting in sharper protruding edges and effective eliminating of low-amplitude structures. The advantage of this method is that it does not depend on local features but instead globally positioning image to suppress the halo. In previous studies [27] [28], it has been demonstrated that the ℓ_0 norm induces stronger sparsity compared to the ℓ_1 and ℓ_2 norms. However, relying solely on the ℓ_0 norm has been found to have limited effectiveness in preventing overfitting of the model. In addition, it is proved in [29] that combining the ℓ_0 norm with additional ℓ_1 or ℓ_2 penalties leads to improved performance. Motivated by these findings, this paper adopts a penalty term that

combines the ℓ_0 and ℓ_2 norms.

In this paper, we propose a dehazing algorithm for a hybrid ℓ_2 - ℓ_0 penalty model based on the atmospheric scattering model and the dark channel principle. This algorithm is inspired by the guided filtering with the ℓ_2 penalty and the ℓ_0 gradient minimization. It weighted sums the coefficients obtained from the ℓ_2 and ℓ_0 penalties, preventing the loss of edge information in sharp regions from the ℓ_2 norm penalty and avoiding an excessively smooth image from the ℓ_0 norm penalty. The model has an update of the guidance image using the ℓ_2 norm penalty. This update includes the initial transmission map obtained by applying the dark channel prior, as well as the new regression coefficient image obtained after applying the ℓ_0 norm penalty to the regression coefficients. The results demonstrate that this model can preserve more detailed information while preserving edges, resulting in higher quality dehazing images.

This paper is organized as follows: the background of the image dehazing is introduced concisely in Section 2; the proposed dehazing scheme is presented in Section 3, followed by the experimental results in Section 4, and Section 5 concludes this work with discussions.

2. Background

2.1. Atmospheric Scattering Model

According to the rule of conservation of energy, the proportion of atmospheric light scattered to the light sensor should be equal to the proportion of the scattered light reflected by the target object [30]. Therefore, by utilizing the physical haze model, a haze-free image can be reconstructed from an image degraded by haze. The model is expressed as:

$$I(x) = J(x)t(x) + A(1-t(x)) \quad (1)$$

where $I(x)$ is the original image, $J(x)$ is the haze-free image, $x=(x,y)$ is the pixel coordinate, A is the atmospheric light, and t is the scene transmission map.

2.2. Estimation of Atmosphere Light

When estimating the atmospheric light value A , a common approach is to select the top 0.1% brightest pixels from the dark channel, mapping them to the input image to identify the corresponding pixel point, and take the maximum value in the RGB channels corresponding to this point as the predicted value for atmospheric light intensity A . However, if the value of A is excessively high, the dehazed image may appear partially distorted, while if it is too low, the image may be overexposed. To enhance the reliability of estimating the atmospheric light, we use the improved quadtree search algorithm proposed in [23].

The atmosphere light is then estimated as

$$A = \text{mean}\left(Q\left(I^{\min}\right), I\right) \quad (2)$$

where $I^{\min} = \min_{c \in \{R, G, B\}}(I^c)$, $Q(I^{\min})$ denotes the quadtree operation using I^{\min} to return the pixel locations for atmosphere light, and $mean(\cdot)$ computes the average of the original pixel values in the atmospheric region.

2.3. Guided Filtering with ℓ_2 Penalty Estimates the Coarse Transmission

He *et al.* [25] proposed using guided filtering to refine the transmission map to optimize the “block effect” caused by an excessively large depth of field during the dehazing process. The key assumption of the guided filter is a local linear model between the guidance image and the filtering output image. The guiding image can either be distinct from or identical to the input image. When the guiding image is identical to the input image, the filtering operation becomes one that preserves edges, which is beneficial for image dehazing. In the proposed method, the initial transmission map t'_i is selected as the same guiding and input images. The linear relationship is shown as:

$$T_i = a_k t'_i + b_k, \forall i \in \omega_k \quad (3)$$

where ω_k is a square window of radius r centered at the pixel k and (a_k, b_k) are linear coefficients assumed to be constant in ω_k , t'_i is the transmission map after refining by the Dark channel prior theory [24], T'_i is the output image.

To ensure the guided image filtering has the best outcome, the difference between the input and output images must be minimized. Consequently, the cost function $E(a_k, b_k)$ uses ℓ_2 norm penalty and defined as follows:

$$\min E(a_k, b_k) = \sum_{i \in \omega_k} [\|T'_i - t'_i\|_2^2 + \varepsilon a_k^2] = \sum_{i \in \omega_k} [\|a_k t'_i + b_k - t'_i\|_2^2 + \varepsilon a_k^2] \quad (4)$$

where ε is a regularization parameter penalizing large, Equation (4) is the linear ridge regression [31] model and its solution is given by

$$a_k = \frac{\sigma_k^2}{\sigma_k^2 + \varepsilon}; b_k = (1 - a_k) \bar{t}'_i \quad (5)$$

where \bar{t}'_i is the mean of t'_i in ω_k , σ_k^2 is the variance of t'_i in ω_k .

2.4. ℓ_0 Gradient Minimization

In guided filtering, the primary benefit of using it as a local filter lies in its capability to preserve the edges of the image while optimizing the “block effect”. However, this filter eliminates halos at the boundaries of the image, which results in the significant edges of the image being penalized, weakened and lost. To address the issue of edge loss during transmission optimization, we introduce the ℓ_0 gradient minimization filter optimization method proposed by Xu *et al.* [26].

Taking the regression coefficient a_k as an example, the established ℓ_0 model is as follows:

$$\min_{a_{\ell_0}} \|a_{\ell_0} - a_k\|_2^2 + \lambda C(a_{\ell_0}) \quad (6)$$

where a_{ℓ_0} is output, a_k is the input of regression coefficient, the regression coefficient b_{ℓ_0} also has the same minimization problem.

$C(a_{\ell_0}) = \#\{p \mid |\partial_x a_{\ell_0}| + |\partial_y a_{\ell_0}| \neq 0\}$ is the gradient measure of a_{ℓ_0} , λ is a weight to control the level of detail. The first term in Equation (6) represents fidelity, while the second term aims to constrain the sparsity of the gradient magnitude of the output.

To solve the objective function, rewrite the objective function as:

$$\min_{a_{\ell_0}, \delta_x, \delta_y} \left\{ \|a_{\ell_0} - a_k\|_2^2 + \lambda C(\delta_x, \delta_y) + \beta \left((\partial_x a_{\ell_0} - \delta_x)^2 + (\partial_y a_{\ell_0} - \delta_y)^2 \right) \right\} \quad (7)$$

where δ is an auxiliary vector to deal with gradient of a_{ℓ_0} and includes two components: δ_x and δ_y , β controls the similarity between δ and gradient of a_{ℓ_0} . Equation (7) is solved through alternatively minimizing (δ_x, δ_y) and a_{ℓ_0} .

3. A New Hybrid ℓ_2 - ℓ_0 Model for Sparse Solutions with Optimizing Transmission Map

To balance the sparsity and the smoothness, the model with hybrid ℓ_2 - ℓ_0 penalty is proposed as follows:

$$T = \mu_1 t_{\ell_2} + \mu_2 t_{\ell_0} \quad (8)$$

where μ_1 and μ_2 are the weight parameters, t_{ℓ_2} is the transmission map obtained by combining regression coefficients after ℓ_2 norm punishment, t_{ℓ_0} is the transmission map obtained by combining the regression coefficients after the ℓ_0 norm penalty.

Initially, we apply ℓ_2 norm penalty to both the guided image I and the input image p , which results in obtaining two regression coefficients (a_k, b_k) :

$$\min E(a_k, b_k) = \sum_{i \in \omega_k} \left[\|T' - p\|_2^2 + \varepsilon a_k^2 \right] = \sum_{i \in \omega_k} \left[\|a_k I + b_k - p\|_2^2 + \varepsilon a_k^2 \right] \quad (9)$$

$$I = p = t'$$

Next, we use these regression coefficients to apply ℓ_0 norm penalty to obtain a_{ℓ_0}, b_{ℓ_0} :

$$\min_{a_{\ell_0}, \delta_x, \delta_y} \left\{ \|a_{\ell_0} - a_k\|_2^2 + \lambda C(\delta_x, \delta_y) + \beta \left((\partial_x a_{\ell_0} - \delta_x)^2 + (\partial_y a_{\ell_0} - \delta_y)^2 \right) \right\} \quad (10)$$

$$\min_{b_{\ell_0}, \delta_x, \delta_y} \left\{ \|b_{\ell_0} - b_k\|_2^2 + \lambda C(\delta_x, \delta_y) + \beta \left((\partial_x b_{\ell_0} - \delta_x)^2 + (\partial_y b_{\ell_0} - \delta_y)^2 \right) \right\}$$

where a_{ℓ_0} and b_{ℓ_0} is smoothed a_k and b_k with ℓ_0 norm, respectively.

Finally, we update the guided image I using the regression coefficients obtained by the ℓ_0 norm penalty, I and p also undergo ℓ_2 norm punishment to obtain a_{ℓ_2}, b_{ℓ_2} :

$$\min E(a_1, b_1) = \sum_{i \in \omega_k} [\|a_{\ell_2} - p\|_2^2 + \varepsilon a_1^2] = \sum_{i \in \omega_k} [\|a_1 I + b_1 - p\|_2^2 + \varepsilon a_1^2]$$

$$a_{\ell_2} = a_1 I + b_1$$

$$I = a_{\ell_0}, p = a_k$$
(11)

$$\min E(a_2, b_2) = \sum_{i \in \omega_k} [\|b_{\ell_2} - p\|_2^2 + \varepsilon a_2^2] = \sum_{i \in \omega_k} [\|a_2 I + b_2 - p\|_2^2 + \varepsilon a_2^2]$$

$$b_{\ell_2} = a_2 I + b_2$$

$$I = b_{\ell_0}, p = b_k$$
(12)

where a_{ℓ_2} is obtained from the ℓ_2 penalty of a_k with a_{ℓ_0} as the guiding image and b_{ℓ_2} is obtained from the ℓ_2 penalty of b_k with b_{ℓ_0} as the guiding image.

Therefore, by combining the outcomes from the aforementioned steps, we arrive at the following result:

$$T = \mu_1 t_{\ell_2} + \mu_2 t_{\ell_0}$$

$$= \mu_1 (a_{\ell_2} * t' + b_{\ell_2}) + \mu_2 (a_{\ell_0} * t' + b_{\ell_0})$$
(13)

After refinement of the transmission map, we transform Equation (1) to obtain the haze-free image J in Equation (14):

$$J(x) = \frac{I(x) - A}{T} + A$$
(14)

For a more intuitive observation of the scheme proposed in this paper, the flow chart is shown in **Figure 1**.

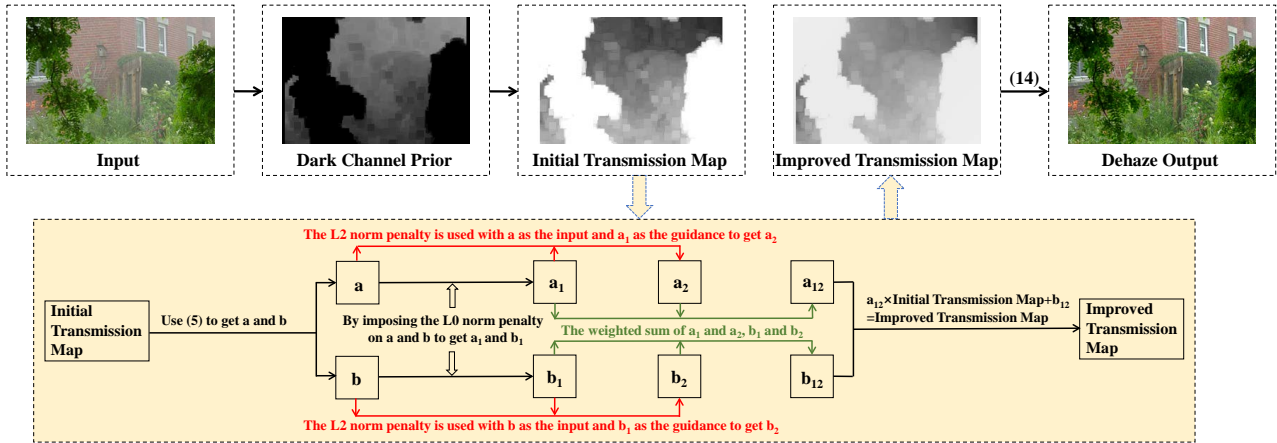


Figure 1. Flow chart of the dehazing proposal.

Figure 2 presents the transmission map and haze-free images obtained through image dehazing using ℓ_2 penalty and combined ℓ_2 - ℓ_0 penalty. The figure clearly demonstrates that increasing the ℓ_0 penalty effectively preserves the obvious edges in the transmission map. Additionally, the resulting haze-free image successfully retains the fine details.

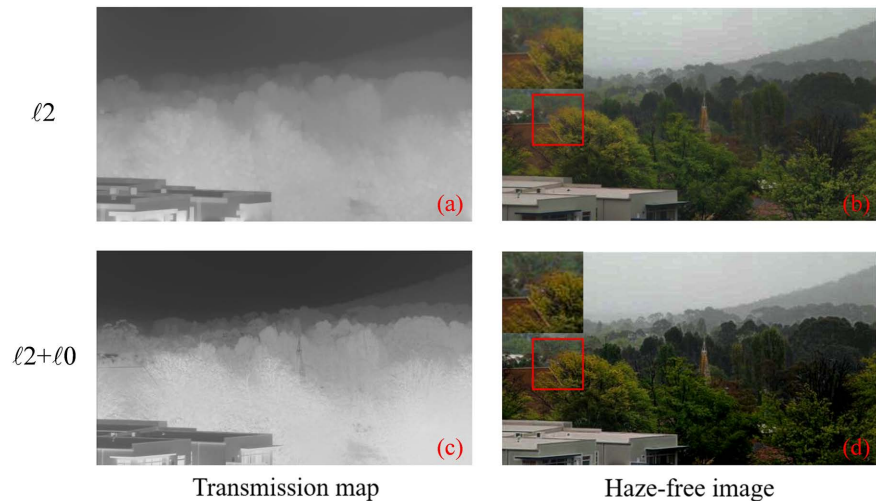


Figure 2. The transmission map and haze-free images obtained by adding different penalty terms, where the upper left image shows a larger picture of the red box. (a) the transmission map obtained by applying ℓ_2 penalty, (b) the haze-free image obtained by applying ℓ_2 penalty, (c) the transmission map obtained by applying ℓ_2 - ℓ_0 penalty, (d) the haze-free image obtained by applying ℓ_2 - ℓ_0 penalty.

4. Experimental Results

To verify the effectiveness of our proposed method, we conduct two sets of experiments. Using the ground truth of the Berkeley segmentation data set [32], we generated synthetic haze images in the first set of simulation experiments with varying haze densities, such as low, medium, and dense haze, by changing the scattering coefficient β in accordance with Equation (15) in accordance with the atmospheric scattering model [33]. We selected three images of varying scenes from the data set and added haze of different densities to conduct the experiment. Additionally, we conducted the second set of experiments using eight real world images that already had haze present in different scenes. Then, we compared it with some various existing dehazing methods, namely, Tarel [11], Meng [12], He [25], RRO [23], Zhu [17], Ralkwar [18], Zhao [19]. In the experiments, the parameters are manually tuned for all methods to ensure the best results.

$$I(x) = J(x)e^{-\beta d(x)} + A(1 - e^{-\beta d(x)}) \quad (15)$$

4.1. Evaluation Criteria

Image quality assessment (IQA) plays a crucial role in detecting the image dehazing effect. It can be categorized into subjective evaluation and objective evaluation. Objective evaluation encompasses various evaluation indicators such as full reference, semi-reference, and no reference [34]-[40]. For synthetic images in the experiment, the performance of image dehazing is evaluated by calculating PSNR, SSIM and CIEDE2000. PSNR [41] measures the distortion between a haze-free image and its ground truth, while SSIM [42] represents the similarity between the ideal and restored images. Higher values of these metrics indicate better dehazing

performance. CIEDE2000 [43] measures color distortion using the Lab color model, with lower scores signify reduced color distortion.

For the real-world images in the experiment, there is without the corresponding ground truth haze-free images, so we use several non-reference image quality evaluation indexes, including contrast, information entropy, average gradient, FADE (Fog Aware Density Evaluator) [44], BIQI (Better Image Quality Index) [45] and Blind Contrast Enhancement Assessment to evaluate [46]. Entropy is a measure of the amount of information in an image, a higher entropy value indicates richer color detail. On the other hand, the contrast value reflects the brightness and clarity of the restored image. Higher contrast values indicate a cleaner image. Additionally, the average gradient represents the ability in recover the image to express the contrast of tiny features. A larger average gradient value signifies more layers within the image and a stronger capacity to express contrasts in fine details, consequently, this results in a clearer image. FADE, a fog-aware density evaluator metric, can assess the visibility of restored images by analyzing the spatial domain deviation between hazy and haze free images, a smaller FADE value indicates a lesser amount of residual haze present in the dehazed result. The BIQI quantifies the quality of distorted images based on perceptual and natural image qualities. A lower score implies a more effective haze removal method. The blind evaluation index is based on the contrast assessment of the visible edges before and after restoration, and it utilizes three descriptors: rate of new visible edges (e), the gain of visibility level (r), and saturated pixel ration (σ). A higher value of e and r indicates a better quality of a dehazed image in terms of preserving edges and enhancing contrast, moreover a smaller value of σ is an indication that the dehazed image has fewer saturated pixels or color distortions compared to the hazy image.

4.2. Synthetic Images

4.2.1. Result

The ground truth is shown in **Figure 3**. **Figures 4-6** display the dehazing results with varying densities of haze added to **Figure 3**. **Table 1** presents the evaluation indicators for three different haze levels in different environments.

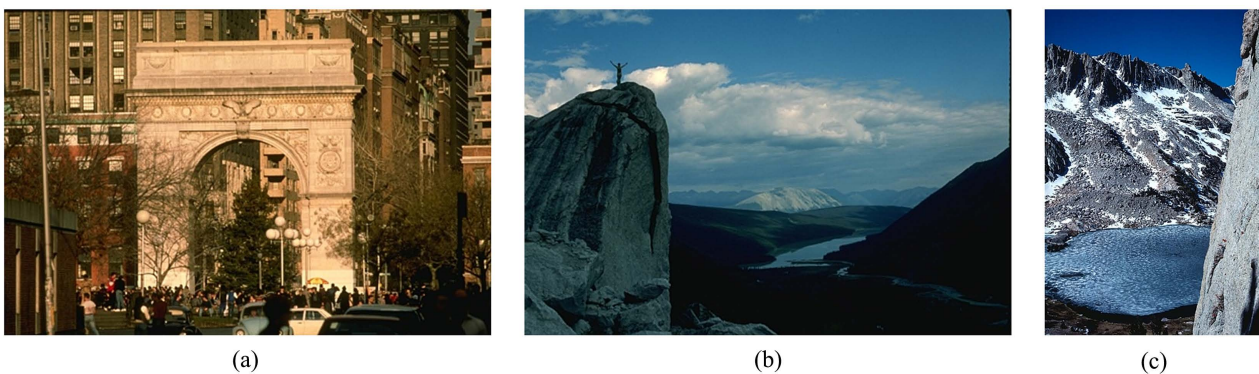


Figure 3. Ground truth (a) **Figure 4**, (b) **Figure 5**, (c) **Figure 6**.

Table 1. Comparison of PSNR, SSIM, CIEDE2000 values with haze condition changes. The 1ST, 2ND winners of each measurement are display with “*” and “♣” respectively.

Metrics	Images	Tarel	Meng	He	RRO	Zhu	Ralkwar	Zhao	Our
PSNR	1	12.0906	14.2276	19.1677♣	17.5710	16.9908	18.5861	17.4758	25.6626*
	2	8.4603	12.8889	11.7310	14.6325♣	14.3163	15.4463	14.0455	20.8745*
	3	6.8901	12.0967	8.0399	12.4654	12.3562	12.4868♣	12.4368	14.8729*
	4	10.5252	15.6673	19.9764	18.0610	14.4334	17.7421	26.9512*	21.7462♣
	5	7.5869	13.6606	14.2213	15.0869	11.8570	13.1387	20.5683*	18.7600♣
	6	6.4291	10.9419	8.9544	12.4301	10.7675	13.5437*	12.6572	12.9107♣
	7	16.8665	12.6900	17.7105	20.1108♣	17.8666	16.1226	19.1245	24.4086*
	8	11.7926	12.1959	18.1033	20.5063♣	15.3091	14.0582	15.9377	22.5254*
	9	8.6035	12.0782	12.3380	17.8191♣	13.2887	13.1885	14.2598	17.8298*
SSIM	1	0.8988	0.9439	0.9781♣	0.9697	0.9591	0.9704	0.9716	0.9962*
	2	0.8198	0.9158	0.9106	0.9473	0.9337	0.9563♣	0.9436	0.9795*
	3	0.7704	0.9077	0.8255	0.9240	0.9138	0.9145	0.9277♣	0.9317*
	4	0.8336	0.9285	0.9733	0.9506	0.9199	0.9701	0.9953*	0.9811♣
	5	0.7601	0.8916	0.9158	0.9232	0.8600	0.8854	0.9763*	0.9650♣
	6	0.7285	0.8549	0.8210	0.8873	0.8364	0.8972♣	0.8874	0.8985*
	7	0.9635	0.9420	0.9830♣	0.9816	0.9729	0.9648	0.9826	0.9941*
	8	0.9062	0.9409	0.9742	0.9876♣	0.9574	0.9518	0.9647	0.9927*
	9	0.8414	0.9285	0.9139	0.9764*	0.9367	0.9330	0.9518	0.9762♣
CIEDE 2000	1	11.0760	12.8238	4.3351	10.9121	8.0194	7.8610♣	10.9879	2.1125*
	2	16.9556	17.2330	9.8924	14.3200	9.5124♣	13.6248	16.4988	3.6882*
	3	20.1291	19.3050	15.7083	15.3984	11.3941♣	16.7263	18.2981	7.4793*
	4	12.8323	7.4279	4.2099	4.9022	9.0671	10.6647	3.8127♣	3.4415*
	5	17.5238	9.4118	7.0856	6.9731	10.4734	11.8321	5.4766♣	4.5197*
	6	19.5586	11.8739	13.3066	9.3310♣	11.8376	13.5734	9.5211	8.6101*
	7	6.8092	9.4979	5.3851	4.7616♣	6.1957	6.4570	5.5694	2.9184*
	8	11.9938	11.1840	5.1680	5.1630♣	7.5016	8.3372	8.3629	3.2086*
	9	16.6186	11.8780	9.6490	6.3003♣	9.0265	10.2918	10.0992	5.5338*

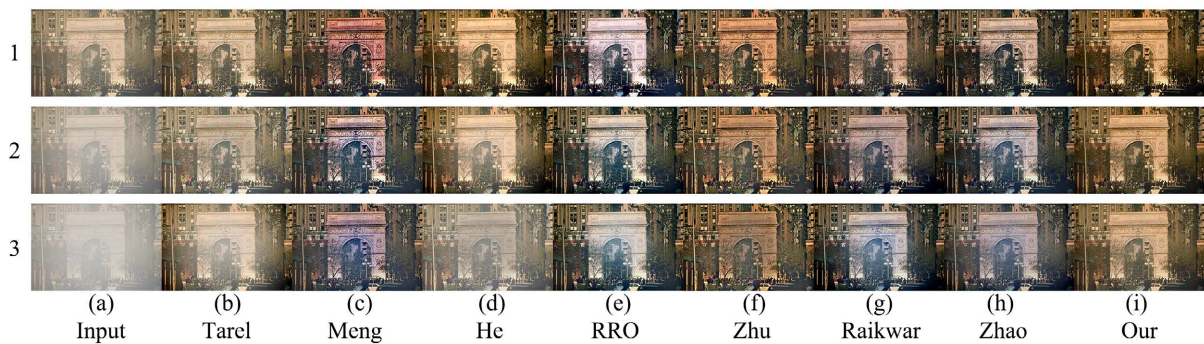


Figure 4. Dehazing results using synthetic images without the sky area: No. 1 shows the low condition, No. 2 shows the medium condition, and No. 3 shows the dense condition. (a) input haze image, (b) Tarel, (c) Meng, (d) He, (e) RRO, (f) Zhu, (g) Raikwar, (h) Zhao, (i) the proposed method.

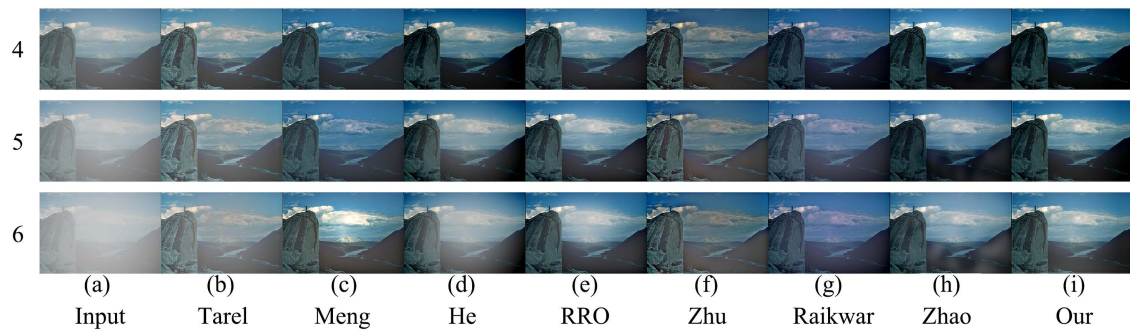


Figure 5. Dehazing results using synthetic images with a large amount of sky area: No. 4 shows the low condition, No. 5 shows the medium condition, and No. 6 shows the dense condition. (a) input haze image, (b) Tarel, (c) Meng, (d) He, (e) RRO, (f) Zhu, (g) Raikwar, (h) Zhao, (i) the proposed method.

The results presented in **Figure 4** indicate a gradual deterioration of the dehazing effect as the level of haze increases. The results of Meng reveal significant color distortion, which can be attributed to the absence of distinct white objects in the image. This led to the selection of only the points closest to white, resulting in the observed phenomenon. The results of Zhu show that as the level of haze deepens, the color of the door demonstrates a progressive darkening. Similarly, the results of Zhao, RRO, and Raikwar show a gradual distortion in the color of the door, with instances of it appearing white and even exhibiting a purple hue.

In **Figure 5**, the results of Tarel indicate that the image still contains significant haze, which worsen as the intensity of haze increases. The results of Meng highlight issues such as oversaturation or excessive darkening of white clouds, possibly due to the selection of different white objects. Both the results of Meng and RRO demonstrate better dehazing outcomes in low to medium haze conditions; but struggle to achieve satisfactory results in denser haze scenarios. The results of Zhu successfully capture mountain textures; however, they also exhibit a general darkening of white cloud colors. The results of Raikwar show noticeable distortion and alteration in the color of white clouds. On the other hand, the results of Zhao perform well in low haze conditions, as indicated in **Table 1**, showing positive indicators. However, as the haze intensifies, white patches become increasingly visible.

In **Figure 6**, the results of Tarel mirror those observed in previous figures, with a significant amount of haze remaining unremoved. The results of Meng display images that are excessively bright in low and medium haze, causing the foreground mountains to lose their original color input, while exhibiting excessively dark colors in dense haze conditions. The results of He indicate a residual amount of haze present during dense haze scenarios. The results of Zhu and Raikwar demonstrate darker images compared to those generated by other comparative algorithms. The results of Zhao highlight increased artifacts and halos on distant mountains as haze levels escalate, accompanied by patches appearing in lakes. The results of RRO exhibit an effective haze removal effect across various degrees of haze, as indicated by the data in **Table 1**, showing very little deviation from the best-performing results.

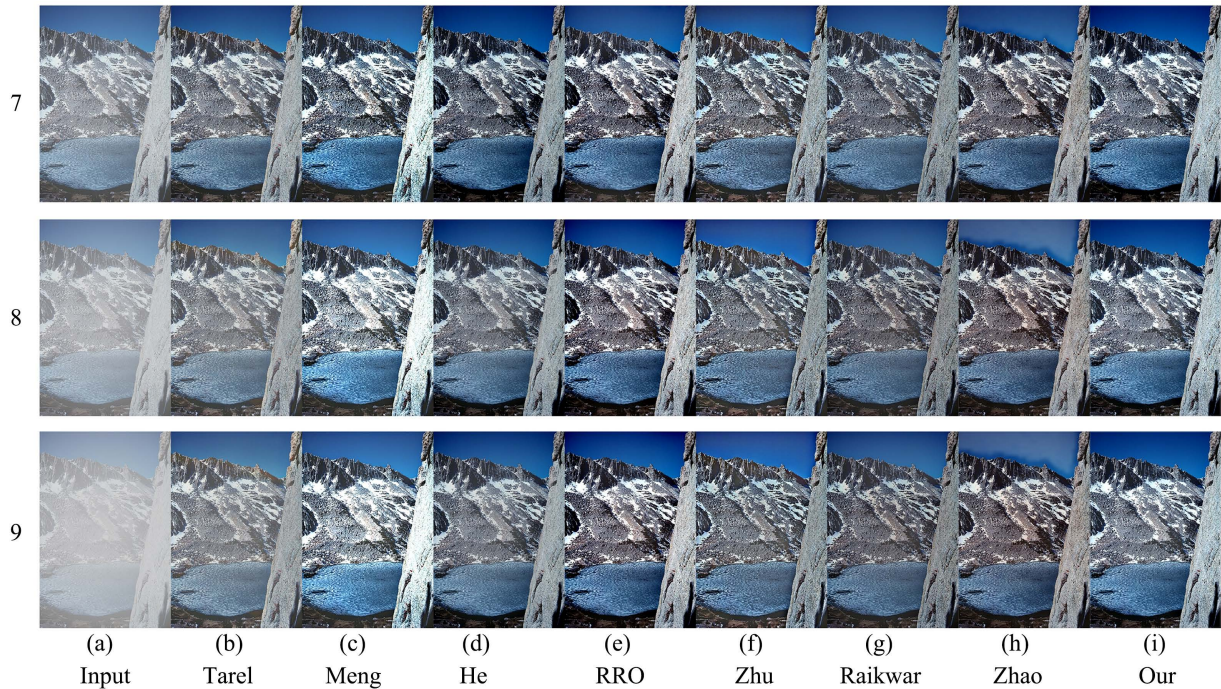


Figure 6. Dehazing results using synthetic images that contain mirror images (e.g., sea surface, lake surface, mirror, etc.): No. 7 shows the low condition, No. 8 shows the medium condition, and No. 9 shows the dense condition. (a) input haze image, (b) Tarel, (c) Meng, (d) He, (e) RRO, (f) Zhu, (g) Raikwar, (h) Zhao, (i) the proposed method.

In contrast, our proposed approach yields better results compared to these competing techniques. It is important to highlight that our approach not only improves the visibility of distant views, but also enhances texture details without altering the original color appearance.

4.2.2. Parameter Sensitivity Analysis

Sensitivity of the weight parameters μ_1 and μ_2 in our algorithm are discussed. In Equation (8), these weight parameters control the balance of the coefficient map after applying the l0 norm penalty and the quadratic ℓ_2 norm penalty. Compared to the other parameters, the weight parameters are more sensitive to PSNR and SSIM. Therefore, we conduct experiments by fixing parameters of $\varepsilon_1, \varepsilon_2, r_1, r_2, \lambda, \beta$ and varying μ_1 and μ_2 , using PSNR and SSIM metrics to measure the accuracy of dehazed results. Here the regularization parameter and the local window radius of the improved guided filter are ε_1 and r_1 ; the regularization parameter and the local window radius of the guided filter with a quadratic limit by the regression coefficient are ε_2 and r_2 , respectively. The sum of μ_1 and μ_2 is 1. **Figure 7** shows the evaluation index values of μ_1 settings in the medium haze density of **Figure 4**. It can be observed that PSNR gradually decreases with the increase of μ_1 , while SSIM presents an upward trend until μ_1 of 0.16, remains stable from 0.16 to 0.19, and then starts to decline after 0.19. Therefore, the parameters as shown in **Table 2** which includes fixed parameters that were carefully chosen after conducting numerous experiments.

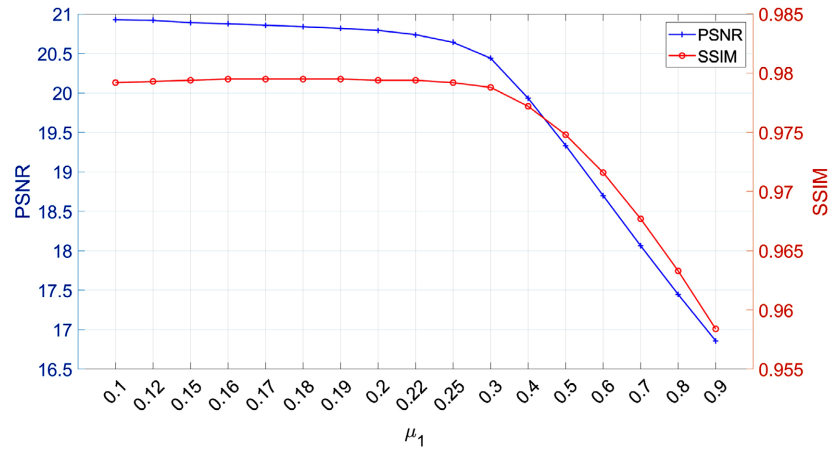


Figure 7. Parameter sensitivity: PSNR and SSIM of our algorithm with respect to the weight μ_1 in the medium haze density of **Figure 4**.

Table 2. Parameters setting of synthetic images.

Parameter	ε_1	r_1	ε_2	r_2	λ	β	μ_1	μ_2
value	2	42	0.01	20	2	0.1	0.16	0.84

4.3. Real World Images

4.3.1. Results

Figure 8 and **Figure 9** show the dehazing results for real world images, and the evaluation indicators of various methods are shown in **Table 3**.

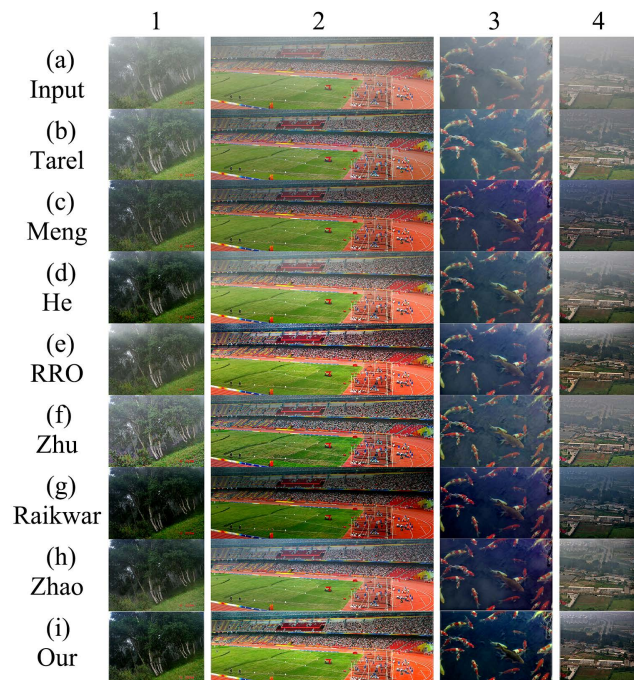


Figure 8. Qualitative comparison of different methods on real world images. (a) input haze image, (b) Tarel, (c) Meng, (d) He, (e) RRO, (f) Zhu, (g) Raikwar, (h) Zhao, (i) the proposed method.

Table 3. Visual quality evaluation using Entropy, Contrast ratio, Mean gradient, FADE, BIQI, σ , e , r . The 1ST, 2ND winners of each measurement are display with “*” and “♣” respectively.

Metrics	Images	Tarel	Meng	He	RRO	Zhu	Ralkwar	Zhao	Our
Entropy	1	6.77	6.43	6.88	6.99♣	7.12*	5.86	6.70	6.79
	2	7.40	7.41	7.55	7.66♣	7.66♣	6.45	7.57	7.70*
	3	7.07♣	6.59	6.84	7.10*	6.78	6.71	6.71	7.00
	4	6.50	6.56	7.29♣	7.18	6.93	6.96	7.08	7.36*
	5	7.33	6.92	7.33	7.48*	7.54	7.17	7.31	7.40♣
	6	7.04	6.81	7.28*	7.15	7.22	7.10	7.03	7.23♣
	7	6.85	6.91	6.71	7.04	7.17	7.25♣	7.29*	7.12
	8	6.79	6.51	7.25	7.43♣	7.28	6.97	7.27	7.44*
Contrast ratio	1	0.37	0.39	0.73	0.55	0.33	1.09*	0.58	0.85♣
	2	0.45	0.53	0.40	0.64♣	0.58	1.01*	0.46	0.62
	3	0.46	0.43	0.42	0.45	0.38	0.80*	0.63	0.71♣
	4	0.34	0.35	0.40	0.53	0.30	0.57♣	0.53	0.62*
	5	0.54	0.47	0.46	0.56♣	0.44	0.46	0.45	0.58*
	6	0.37	0.43	0.46	0.49	0.36	0.61*	0.55♣	0.50
	7	0.42	0.52	0.42	0.53	0.47	0.68*	0.46	0.61♣
	8	0.38	0.35	0.48♣	0.48♣	0.40	0.39	0.30	0.51*
Mean gradient	1	5.78	3.83	6.18	5.40	9.83*	5.72	5.96	7.42♣
	2	11.67	11.53	11.29	17.30♣	17.48*	11.55	12.59	16.13
	3	3.29	2.95	2.84	2.92	3.61*	2.98	3.14	3.53♣
	4	5.10	4.75	4.39	6.31	7.03*	4.93	7.01♣	6.93
	5	11.06	8.82	9.16	10.98	12.29*	8.45	9.72	11.42♣
	6	6.85♣	6.80	5.14	6.11	10.87*	5.42	6.52	5.49
	7	3.13	3.71	4.31	6.46*	4.31	4.00	3.62	5.97♣
	8	4.85♣	4.31	4.38	4.71	6.84*	4.03	3.24	4.66
FADE	1	0.56	0.19	0.21	0.47	0.34	0.14*	0.26	0.15♣
	2	0.24	0.19	0.27	0.14♣	0.15	0.11*	0.22	0.15
	3	0.90	0.75	0.86	0.80	0.65	0.53	0.50*	0.51♣
	4	0.82	0.44	0.84	0.40	0.48	0.29	0.28♣	0.27*
	5	0.20	0.20	0.26	0.19♣	0.31	0.25	0.25	0.15*
	6	0.37	0.26	0.43	0.31	0.25	0.21*	0.22♣	0.34
	7	1.24	0.68	0.92	0.66	0.76	0.57♣	0.68	0.50*
	8	0.79	0.75♣	0.75♣	0.77	0.80	0.94	1.53	0.71*

Continued

BIQI	1	46.42	25.71 [♣]	34.36	38.86	27.25	30.92	34.99	22.10 [*]
	2	21.43 [♣]	25.09	23.22	19.21 [*]	21.60	29.43	25.52	27.96
	3	38.63	40.70	42.81	42.44	37.00 [♣]	41.71	43.44	28.03 [*]
	4	32.25	30.56	30.34	22.56 [*]	23.03 [♣]	28.72	25.61	27.86
	5	19.10	18.41	17.93 [*]	17.96 [♣]	21.01	18.29	18.53	18.24
	6	38.12 [♣]	71.59	45.63	61.36	15.76 [*]	48.09	76.19	47.36
	7	31.09 [♣]	38.18	41.72	35.49	36.11	43.85	50.45	23.23 [*]
	8	27.43	25.99 [♣]	27.10	26.87	37.18	26.18	27.35	25.88 [*]
σ	1	0.00 [*]	95.97	0.92	0.00 [*]	0.00 [*]	7.79	0.00 [*]	0.03 [♣]
	2	0.00 [*]	0.00 [*]	0.00 [*]	0.03	0.18	6.80	0.01 [♣]	0.01 [♣]
	3	0.00 [*]	0.01 [♣]	0.04	0.02	0.02	0.16	0.07	0.00 [*]
	4	0.00 [*]	0.00 [*]	0.09	0.06	0.01 [♣]	0.80	0.31	0.24
	5	0.00 [*]	0.04	0.00 [*]	0.41	0.00 [*]	0.01 [♣]	0.00 [*]	0.01 [♣]
	6	0.00 [*]	0.00 [*]	0.08	0.01 [♣]	0.53	0.49	0.00 [*]	0.85
	7	0.00 [*]	0.00 [*]	0.05	0.03 [♣]	0.00 [*]	0.18	0.21	0.00 [*]
	8	0.00 [*]	0.03 [♣]	1.12	1.02	0.20	0.13	0.00 [*]	0.11
e	1	0.38	-0.54	1.41	1.08	1.37	1.52 [*]	1.51 [♣]	1.51 [♣]
	2	0.21	0.38	0.29	0.34	0.42 [*]	0.40 [♣]	0.35	0.38
	3	0.32	3.35	2.54	2.38	4.75	8.16 [♣]	6.47	8.24 [*]
	4	1.84	3.56	2.24	3.86	3.15	3.88	4.56 [*]	4.43 [♣]
	5	0.37 [*]	0.07	0.07	0.05	0.12 [♣]	0.05	0.08	0.12 [♣]
	6	1.32	2.02 [*]	1.18	1.63	1.56	1.62	1.87 [♣]	1.32
	7	11.65 [*]	5.77	5.39	7.18	6.27	7.36	6.05	8.16 [♣]
	8	1.37 [*]	0.20 [♣]	0.06	0.09	0.04	0.07	0.02	0.20 [♣]
r	1	0.42	6.65	1.80	1.54	2.85 [†]	1.63	1.72	2.22 [♣]
	2	0.50	1.56	1.55	2.34 [♣]	2.54 [*]	1.57	1.73	2.34 [♣]
	3	0.67	1.94	1.85	1.93	2.61 [♣]	1.90	2.09	2.63 [*]
	4	0.71	2.27	2.04	3.01	3.45	2.35	3.62 [♣]	3.74 [*]
	5	0.63	1.33	1.40	1.68	1.89 [♣]	1.27	1.52	1.93 [*]
	6	0.60	2.47 [♣]	1.69	2.14	3.49 [*]	1.86	2.41	1.83
	7	0.99	2.31	2.77	4.32 [♣]	2.70	2.43	2.22	4.43 [*]
	8	0.85	1.40	1.39	1.47	2.24 [*]	1.28	1.02	1.50 [♣]

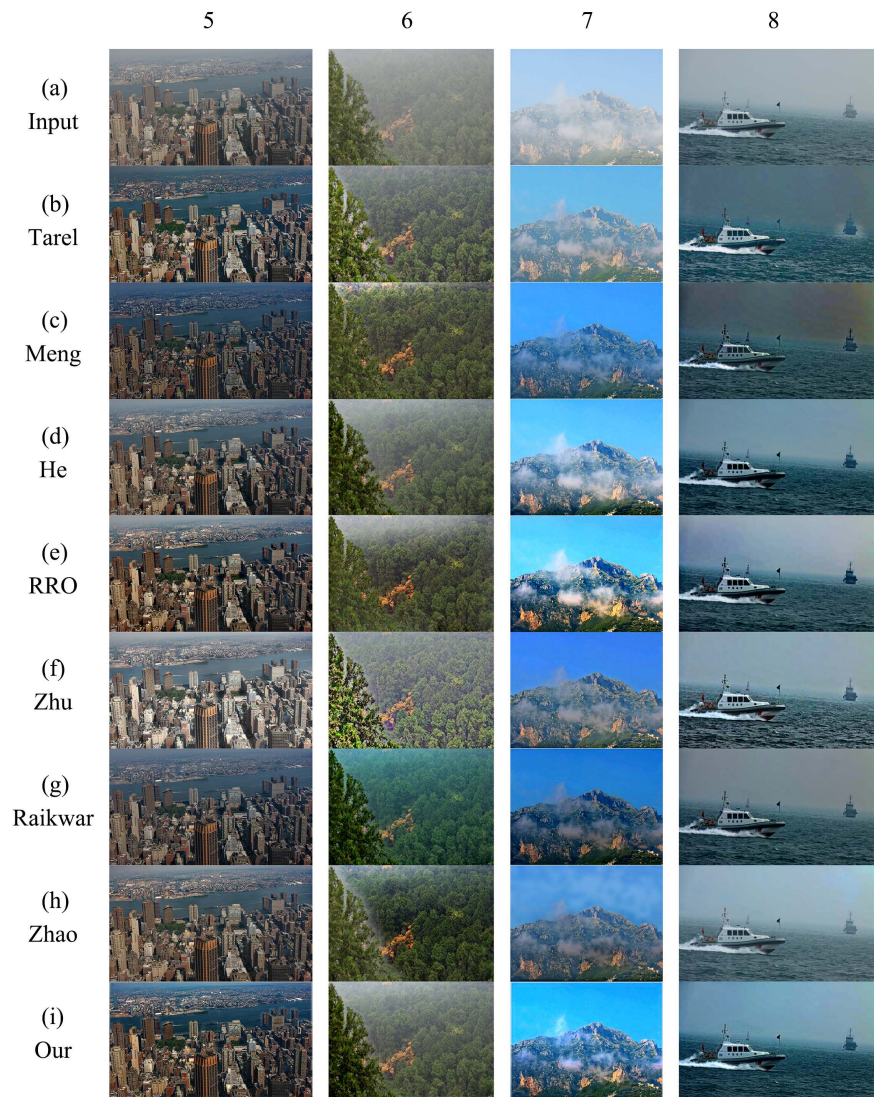


Figure 9. Qualitative comparison of different methods on real world images. (a) input haze image, (b) Tarel, (c) Meng, (d) He, (e) RRO, (f) Zhu, (g) Raikwar, (h) Zhao, (i) the proposed method.

The model of Tarel is not able to completely eliminate the haze effect at Nos. 1, 4 and 6, particularly in the distant areas of Nos. 4 and 6. Additionally, it results in artifact halos on ships in the distant part of No. 8. According to the σ data in **Table 3**, the results of Tarel have little distortion and supersaturated pixels. The results of Meng indicate that the image is too dark in Nos. 3, 4, 5 and 8, and there is distortion in the sky of No. 8. The results of He, RRO and Zhao demonstrate that the details of the scene and objects are well restored, especially in No. 2, according to the data in **Table 3**, it can be seen that the results of RRO seem to have achieved better results in all aspect. However, both the methods of He and RRO still have some haze in the distant part that is not completely removed. Additionally, Nos. 3 and 7 of Zhao exhibit the phenomenon of white spots, and a halo is generated around the tree in the foreground of No. 6. The results of Zhu indicate

a partial distortion in the lower left corner of Nos. 1, 6, and the contrast of No. 5 is too low, resulting in an overall white color for the building. While his objective evaluation indicators perform well according to **Table 3**, his subjective evaluation is not satisfactory. On the other hand, the results of Raikwar generally appear darker compared to others, but they exhibit better haze removal performance, particularly noticeable on Nos. 1 and 2. This is reflected in their high FADE value and Contrast ratio value.

The proposed method in this research has a positive impact on the dehazing effect and color recovery. By applying the ℓ_0 gradient minimization constraint to the ridge regression coefficient based on guided filtering, it better preserves edges, as evidenced by the average gradient and e value in the table.

4.3.2. Parameter Sensitivity Analysis

Here, similar to the parameter sensitivity analysis of the synthetic image, we also conduct experiments by fixing parameters of $\varepsilon_1, \varepsilon_2, r_1, r_2, \lambda, \beta$ and varying μ_1 and μ_2 , using BIQI and e metrics to measure the accuracy of dehazed results. **Figure 10** shows the evaluation index values of μ_1 settings in the No. 3 of **Figure 8**. The figure shows that e generally presents an upward trend, with little difference observed when the μ_1 is between 0.88 and 0.94. Within this interval, the smallest BIQI values are recorded for 0.89 and 0.92. Therefore, we can choose either of these values. The corresponding parameter settings can be found in **Table 4**.

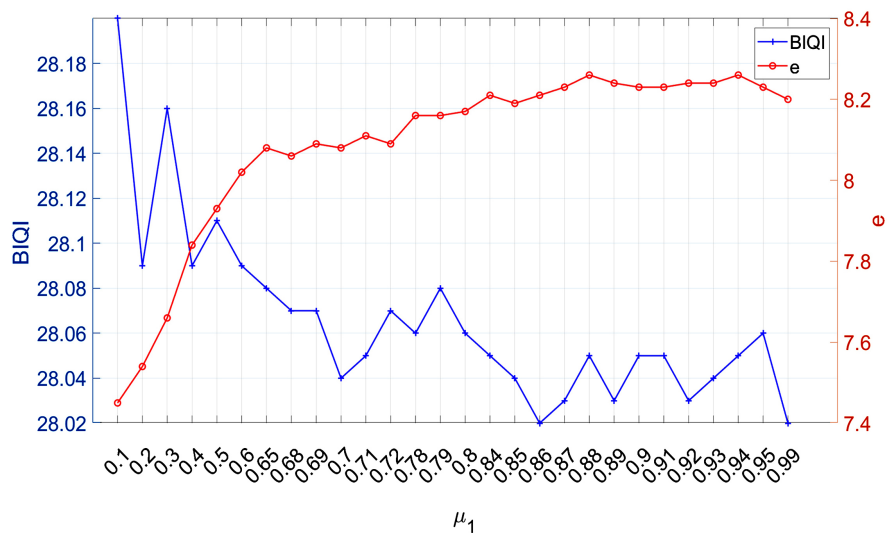


Figure 10. Parameter sensitivity: BIQI and e of our algorithm with respect to the weight μ_1 on the No. 3 of **Figure 8**.

Table 4. Parameter settings of real-world images.

Parameter	ε_1	r_1	ε_2	r_2	λ	β	μ_1	μ_2
value	0.001	4	0.001	10	2	0.004	0.92	0.08

5. Conclusions

To enhance the realism of the existing haze image degradation model, we propose a dehazing model that integrates a hybrid ℓ_2 - ℓ_0 penalization approach. This model refines the transmission map by weighted summation of regression coefficients derived from the ℓ_2 and ℓ_0 penalties. This method effectively smooths out the details while preserving the edges, resulting in a more accurate outline for the refined transmittance map. Consequently, the dehazed image retains more edge information. Experimental results demonstrate that the method proposed in this paper yields favorable outcomes in dehazing both synthetic and real-world images, achieving higher evaluation scores.

In future studies, we plan to enhance the transmission with new regularization terms, and hope to reduce the impact of noise during the dehazing process, resulting in a cleaner and more optimal output image.

Acknowledgements

I would like to express my sincere gratitude to my advisor, Dongjiang Ji, for his invaluable guidance and support throughout this research. His insights and encouragement have been instrumental in shaping my work. I also appreciate the contributions of Chunyu Xu for her assistance in the validation process. Furthermore, I extend my thanks to my colleagues and friends for their encouragement and constructive feedback. This research would not have been possible without their support.

Conflicts of Interest

The authors declare no conflicts of interest regarding the publication of this paper.

References

- [1] Yang, Y. and Wang, Z. (2020) Image Restoration Algorithm Based on Compensated Transmission and Adaptive Haze Concentration Coefficient. *Journal on Communications*, **41**, 66-75.
- [2] Dale-Jones, R. and Tjahjadi, T. (1993) A Study and Modification of the Local Histogram Equalization Algorithm. *Pattern Recognition*, **26**, 1373-1381. [https://doi.org/10.1016/0031-3203\(93\)90143-k](https://doi.org/10.1016/0031-3203(93)90143-k)
- [3] Wang, Q. and Ward, R. (2007) Fast Image/Video Contrast Enhancement Based on Weighted Thresholded Histogram Equalization. *IEEE Transactions on Consumer Electronics*, **53**, 757-764. <https://doi.org/10.1109/tce.2007.381756>
- [4] Stockham, T.G. (1972) Image Processing in the Context of a Visual Model. *Proceedings of the IEEE*, **60**, 828-842. <https://doi.org/10.1109/proc.1972.8782>
- [5] Russo, F. (2002) An Image Enhancement Technique Combining Sharpening and Noise Reduction. *IEEE Transactions on Instrumentation and Measurement*, **51**, 824-828. <https://doi.org/10.1109/tim.2002.803394>
- [6] Land, E.H. (1977) The Retinex Theory of Color Vision. *Scientific American*, **237**, 108-128. <https://doi.org/10.1038/scientificamerican1277-108>
- [7] Jobson, D.J., Rahman, Z. and Woodell, G.A. (1997) Properties and Performance of a

- Center/Surround Retinex. *IEEE Transactions on Image Processing*, **6**, 451-462. <https://doi.org/10.1109/83.557356>
- [8] Rahman, Z., Jobson, D.J. and Woodell, G.A. (1996) Multi-Scale Retinex for Color Image Enhancement. *Proceedings of 3rd IEEE International Conference on Image Processing*, Lausanne, 19 September 1996, 1003-1006. <https://doi.org/10.1109/icip.1996.560995>
- [9] Fattal, R. (2008) Single Image Dehazing. *ACM Transactions on Graphics*, **27**, 1-9. <https://doi.org/10.1145/1360612.1360671>
- [10] Tan, R.T. (2008) Visibility in Bad Weather from a Single Image. 2008 *IEEE Conference on Computer Vision and Pattern Recognition*, Anchorage, 23-28 June 2008, 1-8. <https://doi.org/10.1109/cvpr.2008.4587643>
- [11] Tarel, J. and Hautiere, N. (2009) Fast Visibility Restoration from a Single Color or Gray Level Image. 2009 *IEEE 12th International Conference on Computer Vision*, Kyoto, 29 September-2 October 2009, 2201-2208. <https://doi.org/10.1109/iccv.2009.5459251>
- [12] Meng, G., Wang, Y., Duan, J., Xiang, S. and Pan, C. (2013) Efficient Image Dehazing with Boundary Constraint and Contextual Regularization. 2013 *IEEE International Conference on Computer Vision*, Sydney, 1-8 December 2013, 617-624. <https://doi.org/10.1109/iccv.2013.82>
- [13] Li, Z.G., Zheng, J.H., Zhu, Z.J., Yao, W. and Wu, S.Q. (2015) Weighted Guided Image Filtering. *IEEE Transactions on Image Processing*, **24**, 120-129. <https://doi.org/10.1109/tip.2014.2371234>
- [14] Li, Z. and Zheng, J. (2015) Edge-Preserving Decomposition-Based Single Image Haze Removal. *IEEE Transactions on Image Processing*, **24**, 5432-5441. <https://doi.org/10.1109/tip.2015.2482903>
- [15] Farbman, Z., Fattal, R., Lischinski, D. and Szeliski, R. (2008) Edge-Preserving Decompositions for Multi-Scale Tone and Detail Manipulation. *ACM Transactions on Graphics*, **27**, 1-10. <https://doi.org/10.1145/1360612.1360666>
- [16] Min, D., Choi, S., Lu, J., Ham, B., Sohn, K. and Do, M.N. (2014) Fast Global Image Smoothing Based on Weighted Least Squares. *IEEE Transactions on Image Processing*, **23**, 5638-5653. <https://doi.org/10.1109/tip.2014.2366600>
- [17] Zhu, Z., Wei, H., Hu, G., Li, Y., Qi, G. and Mazur, N. (2021) A Novel Fast Single Image Dehazing Algorithm Based on Artificial Multiexposure Image Fusion. *IEEE Transactions on Instrumentation and Measurement*, **70**, 1-23. <https://doi.org/10.1109/tim.2020.3024335>
- [18] Raikwar, S.C. and Tapaswi, S. (2020) Lower Bound on Transmission Using Non-Linear Bounding Function in Single Image Dehazing. *IEEE Transactions on Image Processing*, **29**, 4832-4847. <https://doi.org/10.1109/tip.2020.2975909>
- [19] Zhao, X. (2021) Single Image Dehazing Using Bounded Channel Difference Prior. 2021 *IEEE/CVF Conference on Computer Vision and Pattern Recognition Workshops (CVPRW)*, Nashville, 19-25 June 2021, 727-735. <https://doi.org/10.1109/cvprw53098.2021.00082>
- [20] Baiju, P.S., Antony, S.L. and George, S.N. (2021) An Intelligent Framework for Transmission Map Estimation in Image Dehazing Using Total Variation Regularized Low-Rank Approximation. *The Visual Computer*, **38**, 2357-2372. <https://doi.org/10.1007/s00371-021-02117-2>
- [21] Yadav, S.K. and Sarawadekar, K. (2023) A New Robust Scale-Aware Weighting-Based Effective Edge-Preserving Gradient Domain Guided Image Filter for Single Image

- Dehazing. *Journal of Signal Processing Systems*, **95**, 475-493. <https://doi.org/10.1007/s11265-023-01849-9>
- [22] Padmini, T.N. and Shankar, T. (2016) De-Hazing Using Guided and L_0 Gradient Minimization Filters. *Indian Journal of Science and Technology*, **9**, 1-6. <https://doi.org/10.17485/ijst/2016/v9i37/102115>
- [23] Shin, J., Kim, M., Paik, J. and Lee, S. (2020) Radiance-Reflectance Combined Optimization and Structure-Guided ℓ_0 -Norm for Single Image Dehazing. *IEEE Transactions on Multimedia*, **22**, 30-44. <https://doi.org/10.1109/tmm.2019.2922127>
- [24] He, K.M., Sun, J. and Tang, X.O. (2011) Single Image Haze Removal Using Dark Channel Prior. *IEEE Transactions on Pattern Analysis and Machine Intelligence*, **33**, 2341-2353. <https://doi.org/10.1109/tpami.2010.168>
- [25] He, K., Sun, J. and Tang, X. (2013) Guided Image Filtering. *IEEE Transactions on Pattern Analysis and Machine Intelligence*, **35**, 1397-1409. <https://doi.org/10.1109/tpami.2012.213>
- [26] Xu, L., Lu, C., Xu, Y. and Jia, J. (2011) Image Smoothing via L_0 Gradient Minimization. *ACM Transactions on Graphics*, **30**, 1-12. <https://doi.org/10.1145/2070781.2024208>
- [27] Dedieu, A., Lázaro-Gredilla, M. and George, D. (2021) Sample-Efficient L_0 - L_2 Constrained Structure Learning of Sparse Ising Models. *Proceedings of the AAAI Conference on Artificial Intelligence*, **35**, 7193-7200. <https://doi.org/10.1609/aaai.v35i8.16884>
- [28] de Resende Oliveira, F.D., Batista, E.L.O. and Seara, R. (2024) On the Compression of Neural Networks Using ℓ_0 -Norm Regularization and Weight Pruning. *Neural Networks*, **171**, 343-352. <https://doi.org/10.1016/j.neunet.2023.12.019>
- [29] Mazumder, R., Radchenko, P. and Dedieu, A. (2023) Subset Selection with Shrinkage: Sparse Linear Modeling When the SNR Is Low. *Operations Research*, **71**, 129-147. <https://doi.org/10.1287/opre.2022.2276>
- [30] Middleton, W.E.K. and Twersky, V. (1954) Vision through the Atmosphere. *Physics Today*, **7**, 21. <https://doi.org/10.1063/1.3061544>
- [31] Kim, J., Jang, W., Sim, J. and Kim, C. (2013) Optimized Contrast Enhancement for Real-Time Image and Video Dehazing. *Journal of Visual Communication and Image Representation*, **24**, 410-425. <https://doi.org/10.1016/j.jvcir.2013.02.004>
- [32] Li, B., Ren, W., Fu, D., Tao, D., Feng, D., Zeng, W., et al. (2019) Benchmarking Single-Image Dehazing and Beyond. *IEEE Transactions on Image Processing*, **28**, 492-505. <https://doi.org/10.1109/tip.2018.2867951>
- [33] Agrawal, S.C. and Jalal, A.S. (2021) Distortion-Free Image Dehazing by Superpixels and Ensemble Neural Network. *The Visual Computer*, **38**, 781-796. <https://doi.org/10.1007/s00371-020-02049-3>
- [34] Min, X., Zhai, G., Gu, K., Zhu, Y., Zhou, J., Guo, G., et al. (2019) Quality Evaluation of Image Dehazing Methods Using Synthetic Hazy Images. *IEEE Transactions on Multimedia*, **21**, 2319-2333. <https://doi.org/10.1109/tmm.2019.2902097>
- [35] Min, X., Zhai, G., Gu, K., Yang, X. and Guan, X. (2019) Objective Quality Evaluation of Dehazed Images. *IEEE Transactions on Intelligent Transportation Systems*, **20**, 2879-2892. <https://doi.org/10.1109/tits.2018.2868771>
- [36] Min, X., Gu, K., Zhai, G., Liu, J., Yang, X. and Chen, C.W. (2018) Blind Quality Assessment Based on Pseudo-Reference Image. *IEEE Transactions on Multimedia*, **20**, 2049-2062. <https://doi.org/10.1109/tmm.2017.2788206>
- [37] Min, X., Zhai, G., Gu, K., Liu, Y. and Yang, X. (2018) Blind Image Quality Estimation

- via Distortion Aggravation. *IEEE Transactions on Broadcasting*, **64**, 508-517. <https://doi.org/10.1109/tbc.2018.2816783>
- [38] Min, X., Gu, K., Zhai, G., Yang, X., Zhang, W., Le Callet, P., *et al.* (2021) Screen Content Quality Assessment: Overview, Benchmark, and Beyond. *ACM Computing Surveys*, **54**, 1-36. <https://doi.org/10.1145/3470970>
- [39] Zhai, G. and Min, X. (2020) Perceptual Image Quality Assessment: A Survey. *Science China Information Sciences*, **63**, Article No. 211301. <https://doi.org/10.1007/s11432-019-2757-1>
- [40] Zhang, J., Min, X., Zhu, Y., Zhai, G., Zhou, J., Yang, X., *et al.* (2022) HazDesNet: An End-To-End Network for Haze Density Prediction. *IEEE Transactions on Intelligent Transportation Systems*, **23**, 3087-3102. <https://doi.org/10.1109/tits.2020.3030673>
- [41] Wang, Z. and Bovik, A.C. (2006) Modern Image Quality Assessment. Springer. <https://doi.org/10.2200/s00010ed1v01y200508ivm003>
- [42] Wang, Z., Bovik, A.C., Sheikh, H.R. and Simoncelli, E.P. (2004) Image Quality Assessment: From Error Visibility to Structural Similarity. *IEEE Transactions on Image Processing*, **13**, 600-612. <https://doi.org/10.1109/tip.2003.819861>
- [43] Sharma, G., Wu, W. and Dalal, E.N. (2004) The CIEDE2000 Color-Difference Formula: Implementation Notes, Supplementary Test Data, and Mathematical Observations. *Color Research & Application*, **30**, 21-30. <https://doi.org/10.1002/col.20070>
- [44] Choi, L.K., You, J. and Bovik, A.C. (2015) Referenceless Prediction of Perceptual Fog Density and Perceptual Image Defogging. *IEEE Transactions on Image Processing*, **24**, 3888-3901. <https://doi.org/10.1109/tip.2015.2456502>
- [45] Moorthy, A.K. and Bovik, A.C. (2010) A Two-Step Framework for Constructing Blind Image Quality Indices. *IEEE Signal Processing Letters*, **17**, 513-516. <https://doi.org/10.1109/lsp.2010.2043888>
- [46] Hautière, N., Tarel, J., Aubert, D. and Dumont, É. (2011) Blind Contrast Enhancement Assessment by Gradient Ratioing at Visible Edges. *Image Analysis & Stereology*, **27**, 87-95. <https://doi.org/10.5566/ias.v27.p87-95>